Journal of Materials Chemistry B

ROYAL SOCIETY OF CHEMISTRY

PAPER

View Article Online
View Journal | View Issue

Cite this: J. Mater. Chem. B, 2025, 13, 8866

Ultrasonic activation of polymer–drug conjugates for targeted and combinational pancreatic cancer therapy†

Dimitra Toumpa, [a] Athina Angelopoulou, [a] Konstantinos Avgoustakis[b] and George Pasparakis *[a]

Received 24th May 2025,
Accepted 12th June 2025

DOI: 10.1039/d5tb01250c

rsc.li/materials-b

In this work, we present a series of polymer–drug conjugates (PDCs) incorporating gemcitabine (GEM) and camptothecin (CPT), linked to polymethacrylate backbones *via* ester and disulfide linkers. Using monomeric prodrug precursors, we employed reversible addition–fragmentation chain transfer (RAFT) polymerization to synthesize colloidally stable PDCs. Upon ultrasound irradiation, these PDCs exhibited accelerated drug release, which was further enhanced by the presence of a sonosensitizer due to reactive oxygen species (ROS) generation. Systematic *in vitro* testing across different treatment modalities revealed formulations capable of outperforming the IC_{50} values of the parent drugs by up to five orders of magnitude. Our findings highlight how the interplay between the PDC structure (*e.g.*, drug combinations and linkers) and ultrasound-triggered activation in the presence of a sonosensitizer significantly enhances the therapeutic potency of these nanomedicines.

1. Introduction

In recent years, remotely activated therapeutic modalities (RATMs) have garnered attention for their ability to enhance the precision and efficacy of cancer drug delivery owing to minimal off-target toxicity and the ability to spatiotemporally modulate drug release at tumor sites.[1–3] RATMs comprise systems that are primarily triggered by magnetic fields, radiofrequencies, light irradiation and ultrasound (US). The complexity of the formulations responding to these external cues can vary from simple administration of drugs in their parent form to more functionally complex micellar vehicles, solid lipid nanoparticles, and mesoporous nanomaterials.[4]

Light activated systems constitute an interesting sub-class of RATMs as they can achieve facile activation by irradiation with red and near infrared wavelengths enabling deep tissue penetration. For example, photodynamic therapy (PDT) utilizes photosensitizers (PS) as prodrugs (usually porphyrin molecules) that can generate cytotoxic reactive oxygen species (ROS) selectively only upon light irradiation.[5–7] PDT can be further enhanced with the co-administration of anticancer drug molecules, which act in a synergistic manner. A variation of this method is photochemical internalization (PCI) where the light dose delivered is of low, sublethal intensity but sufficient enough to induce extensive membrane/organelle photooxidation to increase cell membrane permeability and ultimately cell apoptosis by the increased drug uptake.[8] PCI is far superior compared to PDT in that it can significantly reduce the IC_{50} of the co-administered drug and at the same time enhance the apoptotic to necrotic death ratio, which is beneficial for secondary immune response *in vivo*. Similar therapeutic modalities can be achieved by replacing the light source with an US probe to elicit sonodynamic-type effects. Sonodynamic therapy (SDT) can also be delivered with PSs (now known as sonosensitizers, SSs) and drug molecules for combinational therapies.[9–11] SDT offers the advantage that US probes can potentially cover larger tissue areas; they exert higher versatility in terms of energy that can be delivered and can also be combined with clinically established US imaging (*i.e.*, for image guided drug delivery purposes).

We and others have reported PCI therapeutics with various front-line oncology drugs including vinca alkaloids, taxanes, nucleosides and biologics either in their parent form or formulated as nanomedicines (*i.e.*, drug loaded nanoparticles, polymer drug conjugates *etc.*).[12–16] The exact prerequisites that enhance the IC_{50} of a drug molecule in PCI are relatively elusive as one cannot quantitatively predict the extent of cytotoxicity enhancement of a given drug molecular structure; however, it seems that the interplay of PS/drug confinement, drug lipophilicity, and irradiation timing and dose plays a critical role. These factors can be adjusted by employing nanosized formulations that can co-carry PSs and anticancer drugs in a confined manner.[15]

[a] Department of Chemical Engineering, University of Patras, Patra 26504, Greece. E-mail: gpasp@chemeng.upatras.gr
[b] Department of, Pharmacy, University of Patras, Patra 26504, Greece

† Electronic supplementary information (ESI) available. See DOI: https://doi.org/10.1039/d5tb01250c

In this study we build on previous findings to address key issues that affect the degree of enhancement of IC_{50} of two potent anticancer drugs, namely gemcitabine (GEM) and camptothecin (CPT), in the form of polymer–drug conjugates (PDCs). Although confinement strategies have been reported with physically entrapped micelles or similar systems, the utilization of polymer–drug conjugates as a key RATM component has not been extensively explored despite the distinct formulation advantages that they convey:[17,18] (1) covalent drug attachment that prevents burst release events while allowing for a controlled rate of drug liberation *via* suitable linker chemistries, (2) precise and repeatable drug loading that can be fine-tuned early at the synthesis stage, and (3) the possibility to confine multiple drug molecules and PSs under one polymer scaffold and (4) harness passive targeting capabilities *via* prolonged drug circulation[19] followed by activation only at the site of activation.

Our hypothesis stems from previous findings obtained using PCI protocols where nanoformulation strategies lead to enhanced therapeutic effects. Therefore, it is reasonable to expect similar potency with SDT protocols. By exploring the interplay between different drug and linker combinations and US we perform mechanistic studies on the potency of PDCs against a model pancreatic cell line.

Starting from polymerizable monomer–drug precursors, we employ reversible addition fragmentation chain transfer (RAFT) polymerization from polyethylene glycol chain transfer agents to generate PDCs of different drug molecules attached with two types of linkers, a slow (ester) and a fast (disulfide) hydrolyzing one. The resulting PDCs can be co-activated by an US probe to elicit combinational therapeutic action by confined drug liberation and sensitization. This approach allows for the alteration of drug combinations, linker composition, irradiation dose, and drug loading to optimize the formulation towards IC_{50} minimization. Optimization of the delivery regime, *i.e.*, by adjusting the timing of cells' exposure to sonosensitizers, PDCs and US irradiation, led to the discovery of formulations that either match or even outperform the cytotoxicity of their native-drug counterparts even by several orders of magnitude (Scheme 1).

2. Experimental part

2.1. Materials

4,4′-Azobis(4-cyanovaleric acid) (ACVA), aq. hydrochloride (HCl), magnesium sulfate ($MgSO_4$), sodium bicarbonate ($NaHCO_3$), the macro-chain transfer agent poly(ethylene glycol)-4-cyano-4-(phenylcarbonothioylthio)pentanoate (macro PEG-CTA, M_n = 10 000 g mol^{-1}), pyridine, phthalocyanine (Pc), 1,3-diphenylisobenzofuran (DPBF), zinc acetate dihydrate, tributylamine, terephthalic acid (TA), 5,5′-dithio-bis-(2-nitrobenzoic acid) (DTNB) and dansyl chloride were purchased from Merck. 3,3′-Dithiodipropionic acid, CPT, dimethyl formamide (DMF), dimethylaminopyridine (DMAP), 1-(3-dimethylaminopropyl)3-ethylcarbodiimide hydrochloride (EDCI·HCl), gemcitabine hydrochloride (GEM·HCl), 1-hydroxybenzotriazole (HOBt) formic acid, pyrene and succinic anhydride were purchased from Fluorochem. Dichloromethane (DCM), ethyl acetate (EtOAc), hexane (Hex), 2-hydroxypropyl methacrylate (HPMA), methanol (MeOH), tetrahydrofuran (THF), toluene (PhMe) and *n*-pentanol were supplied by ThermoFisher Scientific. Deuterated chloroform ($CDCl_3$) and deuterated methanol (MeOH-d_4) were purchased from Merck. Ultra-pure three-distilled water (3D-H_2O) was obtained by means of an ELGA Medica R7/15 device. Flash column chromatography (FCC) was performed on Merck silica gel 60 (240–400 mesh, Darmstadt, Germany), and analytical thin layer chromatography (TLC) was performed on Macherey silica gel-F_{254} pre-coated aluminum foils (0.2 mm film).

For the cellular studies in this work, Dulbecco Modified Eagle Medium (DMEM, 1×, Gibco) supplemented with 4.5 g L^{-1} D-glucose, L-glutamine, and pyruvate was used. Phosphate buffered saline, PBS, pH 7.4 (1×, Gibco) and trypsin 0.25%–EDTA in HBSS (biosera) were obtained. 3-[4,5-dimethylthiazol-2-yl]-2,5-diphenyltetrazolium bromide (MTT) and dimethyl sulfoxide (DMSO) for cell culture were purchased from Merck.

2.2. Analytical methods

2.2.1. Nuclear magnetic resonance (NMR). NMR spectroscopy was performed in 5 mm diameter tubes in $CDCl_3$ and d_4-MeOH at 25 °C. ^{1}H NMR spectra were obtained at 600.13 MHz, and ^{13}C NMR spectra at 150.90 MHz on a Bruker AVANCEIII HD spectrometer. The chemical shift values were recorded on the δ scale (expressed in ppm) and the coupling constants (J) in Hertz. The chemical shift scale was calibrated based on the internal solvent signals (δ = 7.24 for $CDCl_3$ and δ = 4.78 for d_4-MeOH). Data were processed using MestReNova software.

2.2.2. Mass spectrometry. High-resolution mass spectra (ESI) were recorded on a Micromass-Platform LC spectrometer.

2.2.3. Size-exclusion chromatography (SEC). SEC was performed using two PLgel MiniMix columns "C" and "D" in series with a refractive index (RI) detector. The eluent was THF with 0.36 wt% of *o*-dichlorobenzene as a flow marker at a flow

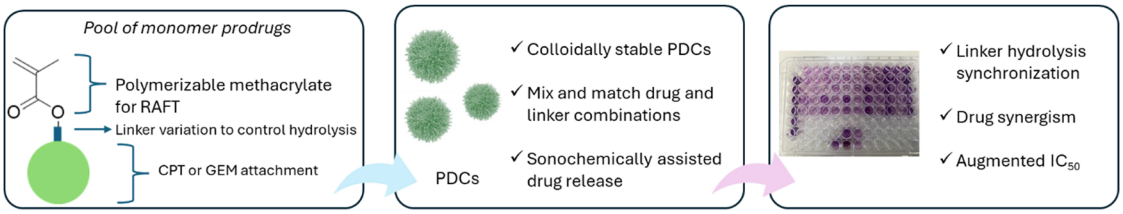

Scheme 1 Our proposed concept of prodrug monomer synthesis that leads to samples with different drug combinations and linker hydrolysis rates with augmented IC_{50} under ultrasound irradiation.

rate of 0.5 mL min^{-1}. The system was calibrated using polystyrene (PS) standards (peak molar masses, M_p = 4000–340 000 g mol^{-1}). This allowed the determination of the number-average molar mass (M_n), the weight-average molar mass (M_w) and the dispersity index ($Đ = M_w/M_n$). All samples were filtered through a nylon membrane with 0.22 μm pore size before injection. Data were collected and processed with Clarity software.

2.2.3. UV-vis spectroscopy. UV absorbance spectra were recorded on an Agilent Technologies Cary 50 UV-vis spectrophotometer in a 200–600 nm range with a cell path length of 10 mm at 25 °C.

2.2.4. Fluorescence spectroscopy. Fluorescence spectra of the samples were recorded on a spectrofluorometer RF-1501 (SHIMADZU) in the 300–600 nm range with a 5-nm slit as the width of the excitation and emission light beams. Each sample was excited at 376 nm and the fluorescence intensity was recorded at 543 nm. A calibration curve at 543 nm was built to determine the concentration.

2.2.5. Dynamic light scattering (DLS). DLS size measurements and zeta-potentials were performed using a zetasizer Brookhaven Instruments Nanobrook Omni. 1 mL of the nanoparticle solution was pipetted into a 1.6 mL disposable cuvette for size measurements and transferred into a folded capillary cell for zeta potential measurements. Data were processed with Matlab.

2.2.6. Transmission electron microscopy (TEM). 5 μL of nanoparticle suspension (1 mg mL^{-1}) kept at 25 °C were deposited on copper grids coated with the Formvar carbon film. The suspension of the samples was left to dry protected in open air. Images were recorded using a JEOL JEM-2010 transmission microscope, operating at 200 kV.

2.2.7. X-ray photoelectron spectroscopy (XPS). XPS measurements were carried out in an ultra high vacuum (UHV) chamber, which has been previously described in detail,[20] operated at a pressure of 3×10^{-9} mbar. Briefly, the XP spectra were recorded using a non-monochromatic AlKa excitation source (1486.6 eV) at setting of 12 kV anode potential and 20 mA emission current, and an electron energy analyzer (Leybold LH EA11) was operated at 100 eV pass energy, while quoted binding energies are accurate to 0.1 eV. The sample powder was deposited onto a thin lead sheet and the under-analysis area was a 2×5 mm^2 rectangle. Surface atomic ratios were calculated *via* appropriate experimental relative sensitivity factors (Wagner experimental RSF database corrected for the analyzer transmission function).[21]

2.3. Synthesis procedures

2.3.1. Synthesis of the slow-reducible linker (HPMA-Suc). To a solution of HPMA (721 mg, 5 mmol, 100 mL round bottom flask) and DMAP (733 mg, 6 mmol) in DCM (30 mL), succinic anhydride (676 mg, 6.76 mmol) was added. The reaction was left under magnetic stirring at 35 °C overnight under N_2 stirring. After the completion of the reaction (monitored by TLC), the mixture was diluted with DCM, washed with 1 N HCl and brine, dried over $MgSO_4$, filtered, and evaporated to dryness under vacuum. The residue was subjected to FCC, using the solvent system Hex/EtOAc 6 : 4 as the eluent, to give a pure product as a white solid (90%); R_f (Hex/EtOAc 6 : 4): 0.30; ^{1}H NMR ($CDCl_3$, 600 MHz) δ 1.23 (d, J = 6.54 Hz, 3H), 1.88 (s, 3H), 2.54–2.64 (m, 4H), 4.07–4.13 (m, 1H), 4.19 (dt, J = 3.54 & 4.56 Hz, 1H), 5.12–5.20 (m, 1H), 5.53 (dt, J = 1.5 & 5.46 Hz, 1H), 6.05 (d, J = 6.9 Hz, 1H), 9.83 (br s, 1H) ppm; ^{13}C NMR ($CDCl_3$, 151 MHz) δ 16.33, 18.13, 28.83, 28.97, 66.17, 68.55, 126.06, 135.82, 167.07, 171.47, 177.82 ppm.

2.3.2. Synthesis of the slow-reducible CPT prodrug (HPMA-Suc-CPT). To a solution of HPMA-Suc (30 mg, 0.12 mmol) and EDCI·HCl (57.5 mg, 0.3 mmol) in DCM (2.25 mL), was added CPT (20 mg, 0.057 mmol) and DMAP (6.2 mg, 0.051 mmol). The reaction was left at room temperature overnight stirring under N_2. After the completion of the reaction (monitored by TLC), the mixture was diluted with DCM, washed with 5% aq. $NaHCO_3$, H_2O and brine, dried over $MgSO_4$, filtered and evaporated to dryness under vacuum. The residue was subjected to FCC, using the solvent system Hex/EtOAc 2 : 8 as the eluent, to give pure product as a yellow solid (80.9%); R_f (Hex/EtOAc 2 : 8): 0.23; ^{1}H NMR ($CDCl_3$, 600 MHz) δ 0.98 (t, J = 7.44 Hz, 3H), 1.13–1.26 (m, 3H), 1.87 (t, J = 13.86 Hz, 3H), 2.11–2.17 (m, 1H), 2.22–2.29 (m, 1H), 2.59–2.68 (m, 2H), 2.79–2.90 (m, 2H), 3.98–4.21 (m, 2H), 5.04–5.18 (m, 1H), 5.26 (d, J = 5.34 Hz, 2H), 5.38 (d, J = 17.1 Hz, 1H), 5.51 (t, J = 21.84 Hz, 1H), 5.66 (dd, J = 3 & 14.04 Hz, 1H), 6.05 (dd, J = 16.68 & 6.72 Hz, 1H), 7.30–7.33 (m, 1H), 7.66 (t, J = 7.5 Hz, 1H), 7.83 (t, J = 7.98Hz, 1H), 7.93 (d, J = 8.1 Hz, 1H), 8.24 (d, J = 8.52 Hz, 1H), 8.39 (s, 1H) ppm; ^{13}C NMR ($CDCl_3$, 151 MHz) δ 7.50, 16.30, 18.20, 28.83, 31.73, 49.92, 65.97, 66.99, 68.69, 76.26, 96.55, 120.18, 126.01, 128.08, 128.22, 128.53, 128.57, 129.33, 130.77, 131.40, 135.77, 145.93, 145.98, 148.51, 152.19, 157.31, 166.91, 167.31, 171.05, 171.22 ppm; ESI-MS (30 eV) m/z: $[M + H]^+$ calcd for $C_{31}H_{29}N_2O_9^+$ 574.20, found 575.32, $[M + Na]^+$ calcd for $C_{31}H_{30}N_2NaO_9^+$ 597.18, found 597.30, $[M + K]^+$ calcd for $C_{31}H_{30}KN_2O_9^+$ 613.16, found 613.62.

2.3.3. Synthesis of the slow-reducible GEM prodrug (HPMA-Suc-GEM). To a solution of GEM·HCl (30 mg, 0.10 mmol) in DMF (1.2 mL), was added HOBt (13.5 mg, 0.10 mmol), EDCI·HCl (19.17 mg, 0.10 mmol), pyridine (92 μL, 1.18 mmol) and HPMA-Suc (24.9 mg, 0.10 mmol). The reaction was left to be stirred at room temperature for 72 h under N_2. After the completion of the reaction (monitored by TLC), the mixture was diluted with EtOAc, washed with 5% aq. $NaHCO_3$, H_2O and brine, dried over $MgSO_4$, filtered and evaporated to dryness under vacuum. The residue was subjected to FCC, using the solvent system DCM/MeOH 15 : 1 as the eluent, to give pure product as a white solid (39.2%); R_f (DCM/MeOH 15 : 1): 0.11; ^{1}H NMR ($CDCl_3$, 600 MHz) δ 1.27 (d, J = 6.48 Hz, 3H), 1.90 (s, 3H), 2.68 (s, 3H), 2.83–2.92 (m, 2H), 3.89 (d, J = 10.8 Hz, 1H), 3.99–4.04 (m, 2H), 4.11–4.15 (m, 1H), 4.19–4.23 (m, 1H), 4.61 (s, 1H), 5.15–5.19 (m, 1H), 5.55 (d, J = 6.42 Hz, 1H), 6.07 (d, J = 6.6 Hz, 1H), 6.11–6.14 (m, 1H), 7.40 (s, 1H), 8.13 (s, 1H) ppm; ^{13}C NMR ($CDCl_3$, 151 MHz) δ 16.40, 18.18, 28.08, 31.98, 59.72, 66.13, 68.89, 87.71, 97.68, 122.51, 125.94, 126.23, 135.82, 136.17, 167.13, 172.27, 172.60 ppm; ESI-MS (30 eV) m/z: $[M + H]^+$ calcd for $C_{20}H_{25}F_2N_3O_9^+$ 490.16, found 490.40,

$[M + Na]^+$ calcd for $C_{20}H_{25}F_2N_3NaO_9^+$ 512.14, found 512.30, $[M + K]^+$ calcd for $C_{20}H_{25}F_2KN_3O_9^+$ 528.12, found 528.40.

2.3.4. Synthesis of the fast-reducible linker (HPMA-SS). To a solution of HPMA (1.35 g, 9.39 mmol) and 3,3′-dithiodipropionic acid (1.88 g, 8.92 mmol) in DCM (37.6 mL), was added DMAP (160.6 mg, 1.31 mmol). Then, a solution of EDCI·HCl (1.8 g, 9.39 mmol) in DCM (18.8 mL) was added dropwise at the reaction mixture at 0 °C. The reaction was left to be stirred at room temperature overnight under N_2. After the completion of the reaction (monitored by TLC), the mixture was diluted with DCM, washed with 1N HCl, H_2O and brine, dried over $MgSO_4$, filtered and evaporated to dryness under vacuum. The residue was subjected to FCC, using the solvent system PhMe/EtOAc 8 : 2 as the eluent, to give pure product as a colorless oil (49.2%); R_f (PhMe/EtOAc 8 : 2): 0.24; ^{1}H NMR ($CDCl_3$, 600 MHz) δ 1.29 (d, J = 6.54 Hz, 3H), 1.94 (s, 3H), 2.72–2.80 (m, 4H), 2.91–2.93 (m, 4H), 4.12–4.17 (m, 1H), 4.22–4.26 (m, 1H), 5.19–5.25 (m, 1H), 5.59 (dt, J = 1.5 & 8.34 Hz, 1H), 6.11 (d, J = 7.14 Hz, 1H) ppm; ^{13}C NMR ($CDCl_3$, 151 MHz) δ 16.62, 18.39, 32.88, 33.25, 33.94, 34.35, 66.32, 68.90, 126.29, 136.02, 167.18, 171.16, 177.27 ppm.

2.3.5. Synthesis of the fast-reducible CPT prodrug (HPMA-SS-CPT). To a solution of HPMA-SS (50 mg, 0.1049 mmol) in DCM (2.79 mL), was added EDCI·HCl (71.5 mg, 0.373 mmol), CPT (24.6 mg, 0.071 mmol) and DMAP (7.7 mg, 0.063 mmol). The reaction was left to be stirred at room temperature overnight under N_2. After the completion of the reaction (monitored by TLC), the mixture was diluted with DCM, washed with H_2O and brine, dried over $MgSO_4$, filtered and evaporated to dryness under vacuum. The residue was subjected to FCC, using the solvent system Hex/EtOAc 2 : 8 as the eluent, to give pure product as a yellow oil (46%); R_f (Hex/EtOAc 2 : 8): 0.26; ^{1}H NMR ($CDCl_3$, 600 MHz) δ 0.99 (t, J = 7.44 Hz, 3H), 1.24 (q, J = 6.06 Hz, 3H), 1.91 (s, 3H), 2.13–2.19 (m, 1H), 2.26–2.32 (m, 1H), 2.69–2.72 (m, 2H), 2.87–2.96 (m, 6H), 4.06–4.20 (m, 2H), 5.12–5.20 (m, 1H), 5.28 (s, 2H), 5.40 (d, J = 14.04 Hz, 1H), 5.54–5.56 (m, 1H), 5.67 (d, J = 17.1 Hz, 1H), 6.08 (d, J = 6.6 Hz, 1H), 7.28 (s, 1H), 7.67 (td, J = 1.02 & 6 Hz, 1H), 7.83 (td, J = 1.32 & 5.52 Hz, 1H), 7.94 (d, J = 7.92 Hz, 1H), 8.23 (d, J = 8.25 Hz, 1H), 8.40 (s, 1H) ppm; ^{13}C NMR ($CDCl_3$, 151 MHz) δ 7.58, 16.44, 18.24, 31.78, 32.42, 33.10, 33.77, 34.18, 49.96, 66.12, 67.09, 68.63, 76.31, 96.29, 120.28, 126.07, 128.09, 128.20, 128.51, 129.51, 130.76, 131.31, 135.86, 145.67, 146.15, 148.69, 152.22, 157.31, 166.93, 167.31, 170.72, 170.92 ppm; ESI-MS (30 eV) m/z: $[M + H]^+$ calcd for $C_{33}H_{35}N_2O_9S_2^+$ 667.18, found 667.21, $[M + Na]^+$ calcd for $C_{33}H_{34}N_2NaO_9S_2^+$ 689.16, found 689.50, $[M + K]^+$ calcd for $C_{33}H_{34}KN_2O_9S_2^+$ 705.13, found 705.43 $[M + K]^+$.

2.3.6. Synthesis of the fast-reducible GEM prodrug (HPMA-SS-GEM). To a solution of GEM·HCl (154.6 mg, 0.516 mmol) in DMF (6.20 mL), was added HOBt (69.7 mg, 0.516 mmol), EDCI·HCl (98.9 mg, 0.516 mmol), pyridine (490 μL, 6.08 mmol) and HPMA-Suc (173.6 mg, 0.516 mmol). The reaction was left to be stirred at room temperature for 72 h under N_2. After the completion of the reaction (monitored by TLC), the mixture was diluted with EtOAc, washed with 5% aq. $NaHCO_3$, H_2O and brine, dried over $MgSO_4$, filtered and evaporated to dryness under vacuum. The residue was subjected to FCC, using the solvent system DCM/MeOH 15 : 1 as the eluent, to give pure product as a white solid (66.6%); R_f (DCM/MeOH 15 : 1): 0.07; ^{1}H NMR ($CDCl_3$, 600 MHz) δ 1.29 (d, J = 6.42 Hz, 3H), 1.93 (s, 3H), 2.72–2.76 (m, 2H), 2.91–2.99 (m, 6H), 3.93 (d, J = 11.34 Hz, 1H), 4.03 (dd, J = 4.44 & 19.02 Hz, 2H), 4.12–4.16 (m, 1H), 4.21–4.25 (m, 1H), 4.49 (s, 1H), 5.19–5.22 (m, 1H), 5.59 (d, J = 8.34 Hz, 1H), 6.10 (d, J = 6.66 Hz, 1H), 6.18 (s, 1H), 7.46 (s, 1H), 8.49 (s, 1H) ppm; ^{13}C NMR ($CDCl_3$, 151 MHz) δ 16.50, 18.25, 32.13, 32.99, 33.87, 34.16, 59.11, 66.12, 68.82, 82.20, 85.49, 96.99, 120.66, 122.39, 125.96, 126.25, 135.85, 136.20, 168.88, 167.10, 171.23, 171.56 ppm; ESI-MS (30 eV) m/z: $[M + H]^+$ calcd for $C_{22}H_{30}F_2N_3O_9S_2^+$ 582.14, found 582.31, $[M + Na]^+$ calcd for $C_{22}H_{29}F_2N_3NaO_9S_2^+$ 604.12, found 604.29, $[M + K]^+$ calcd for $C_{22}H_{29}F_2KN_3O_9S_2^+$ 620.09, found 620.16 $[M + K]^+$.

2.3.7. General procedure of the RAFT polymerization of the prodrugs (D_p = 50). In a 10 mL one-neck round-bottom flask, prodrug (0.075 mmol, 50 eq.), macroPEG-CTA M_n = 10 000 g mol^{-1} (25 mg, 0.0015 mmol, 1 eq.) and ACVA (0.1 mg, 0.000375 mmol, 0.25 eq.) were dissolved in anhydrous DMF (0.425 mL). The flask was sealed with a rubber septum and purged using N_2 for 15 min. The flask was heated at 70 °C for 24 h under magnetic stirring. The reaction was stopped by exposing the solution to open air and the polymer/monomer mixture was precipitated using diethyl ether. The residual monomer was washed away repeating this procedure two more times and the polymer was dried under vacuum. All purified polymers were analyzed with SEC (Fig. S5, ESI†) and NMR (Fig. S1–S4, ESI†).

2.3.8. Synthesis of Zn-phthalocyanine (ZnPc). ZnPc was prepared according to a previously reported procedure.[22] In a solution of Pc (500 mg, 0.97 mmol) and zinc acetate dihydrate (445 mg, 2.425 mmol) in n-pentanol (73 mL), was added tributylamine (11.5 mL, 48.5 mmol). Metalation requires an organic base to remove the acidic protons from the center of the Pc ring. The reaction mixture was heated for 2 h at 160 °C under N_2 and then cooled down at room temperature. The dark colored mixture was filtered at ambient temperature, giving a dark-colored cake. At the end of the reaction, any excess base is easily removed by washing with dilute HCl, and thus the reaction mixture was washed first with H_2O, then with 0.6 M HCl, again with H_2O and finally with EtOH. The dark powder was dried in open air, yielding 87 mol% based on Pc. Pure ZnPc was analyzed with UV-vis and XPS to confirm the insertion of the Zn center (see ESI,† for analysis and Fig. S28).

2.4. Formulation

2.4.1. Critical aggregation concentration (CAC). The CAC of the polymers was studied using the standard pyrene protocol.[23] In order to determine the CACs, the absorbance I_1 (309 nm)/I_3 (339 nm) of the pyrene in UV-vis spectra was plotted against the log of concentration. Independent linear regressions were performed on the observed data points above and below the evident CAC. Finally, the CACs were derived from the intersection points of the independent linear regressions. Prior to the measurements, a pyrene stock solution of 0.6 μM in

phosphate buffered saline (PBS) was freshly prepared by dissolving the probe in acetone. Increasing concentrations of the amphiphiles (from 0.001 to 2 mg mL^{-1}) were added to pyrene (0.6 μM) from a stock solution, and absorption spectra were recorded at different amphiphile concentrations. All samples were stirred thoroughly by using a laboratory vortex shaker to ensure proper mixing and dissolution of the compounds. All measurements were carried out at 25 ± 2 °C and were taken using a UV-vis spectrometer. Data analysis was performed using Matlab software (Fig. S6 and S7, ESI†).

2.4.2. Nanoparticle preparation. Polymer conjugates, each block-copolymer (1 mg) was dissolved in a $CHCl_3/H_2O$ mixture (1 : 1 v/v) in a sample vial with a total volume of 2 mL and the organic phase was evaporated in a controlled manner using a rotor evaporator. The vial was immersed in a water bath at 40 °C and was rotated at a constant speed of 100 rpm under a pressure of 100 mbar, until constant weight was achieved. The nanoparticles were characterized using DLS and TEM. Data analysis was performed using Matlab software. The same protocol was followed to form the PDC combinations by mixing different polymers at 1 : 1 (*i.e.*, GEM: CPT) drug molar stoichiometry.

2.4.3. Stability of the nanoparticles. The nanoparticle suspension samples were left at room temperature. After 10 days, the size and dispersity were measured using DLS. Data analysis was performed using Matlab software.

2.5. US treatment

For the US treatment we used the SONIDEL SP300 sonoporator. To expose the samples to US, water was added to a Petri dish containing the sample vials or cell well-plates, serving as the medium for ultrasound wave transmission. The US exposure parameters used are as follows: 1 MHz frequency, 25% duty cycle, and a pulse repetition frequency of 100 Hz. The intensities and exposure times ranged from 1.00 to 4.00 W cm^{-2} for 30 sec to 5 min, respectively.

2.6. Evaluation of US-mediated ROS production

2.6.1. DPBF assay. To determine the potential of the phthalocyanines to produce singlet oxygen under US stimulation we utilized the photo-oxidation of 1,3-diphenylisobenzofuran (DPBF) as a quantitative method.[24] Specifically, 2 mL of the photosensitizer suspension in water was added to an aerated solution of DPBF (10 μM) in an $EtOH/H_2O$ 1 : 1 solvent system. The solution was then irradiated with US emitting at a frequency of 1 MHz, using a power density of 4 W cm^{-2} for 60 min and a 25% duty cycle at a pulse repetition frequency of 100 Hz. This procedure was repeated for the DPBF solution in the absence of photosensitizer and for a deoxygenated DPBF solution containing the photosensitizer. Aliquots were taken ever 5 min and with a UV-vis spectrometer the DPBF absorbance at 410 nm was recorded. Measurements were taken in triplicate and data were analyzed using Matlab software.

2.6.2. $^{\bullet}OH$ radicals. The presence of $^{\bullet}OH$ was determined using terephthalic acid (TA).[25] In an aqueous solution of 0.5 mM NaOH, TA was added for achieving a final concentration of 2 mM. The photosensitizer was dissolved in 10 μL of DMSO and then H_2O was added to reach the concentration of 2 mM. The two solutions were mixed and then irradiated with US emitting at a frequency of 1 MHz, using a power density of 4 W cm^{-2} for 60 min and a 25% duty cycle at a pulse repetition frequency of 100 Hz. This procedure was repeated for the TA solution in the absence of photosensitizer. Aliquots were taken every 5 min and with a UV-vis spectrometer the 2-hydroxyterephthalic acid (HTA) absorbance at 310 nm was recorded. Measurements were taken in triplicate and data were analyzed using Matlab software.

2.6.3. Ellman's assay. The dissociation of the disulfide bridges and the formation of thiol groups as a function of US (or US combined with Pc/ZnPc) was determined using Ellman's assay.[26] Specifically, 1 mg mL^{-1} of the PDC in PBS (pH 7.4) was irradiated with US emitting at a frequency of 1 MHz, using a power density of 4 W cm^{-2} for 60 min and a 25% duty cycle at a pulse repetition frequency of 100 Hz. Aliquots were taken every 5 min and 50 μL of Ellman's suspension (4 mg mL^{-1} in PBS pH 7.4) was added in each sample and the pH was quenched to pH 8, if necessary, with a solution of 0.05 mM NaOH. Then absorbance at 412 nm was recorded with a UV-vis spectrometer. Measurements were taken in triplicate and data were analyzed using Matlab software.

2.7. Drug release studies

2.7.1. CPT release studies monitored by LC-MS/MS. To determine CPT release kinetics, suspensions of the nanoparticle's samples were prepared in water at a concentration of 1 mg mL^{-1} as previously described and they were transferred to a dialysis bag of 3500 kDa MWCO, which was immersed in 3 mL of PBS of pH 7.4 or pH 5.5 (to mimic the acidic endosome compartments), at 37 °C. At predetermined time intervals (30 min, 1 h, 2 h, 4 h, 6 h, 18 h and 24 h), all of the medium was collected and immediately replaced with fresh medium. To evaluate the US effect the experiments were repeated using US after 1 h with a frequency of 1 MHz, a duty cycle of 25% (pulse frequency = 100 Hz) for 5 min and an ultrasound power density of 1.00 and 3.00 W cm^{-2}, or for 30 sec and ultrasound power densities of 2.00 and 4.00 W cm^{-2}. The collected aliquots were diluted with acetonitrile and formic acid in an H_2O/ACN/formic acid ratio of 1 : 1 : 0,01, and the released drug was quantified by LC-MS/MS. Chromatographic analysis was performed on a Waters HPLC system (Alliance HT 2795) equipped with a temperature-controlled autosampler and a degasser. Chromatographic separation was achieved using a Waters BEH C18 column (2.1 mm × 50 mm, 1.7 μm, Waters Corp., MA, USA), with a flow rate of 0.3 mL min^{-1} for a mobile phase consisting of H_2O (solvent A) and acetonitrile (solvent B). The column temperature was maintained at 40 °C throughout all the experiments, while the sample temperature was kept at 10 °C in the autosampler tray. The sample (50 μL) was injected for analysis, and the gradient started immediately after the injection. The elution program was as follows: solvent B was initially equilibrated at 10%, linearly increased from 10% to 50% within 2 min, linearly increased from 50% to 90% in 5 min, kept stable

at 90% for 1 min, then decreased at 10% in 1 min, and kept stable at 10% for 4 min. The total data acquisition duration was 13 min.[27] The HPLC system was coupled with a Micromass Quattro Micro tandem MS system equipped with a quadrupole analyzer and an electrospray ion source that operated in positive ion mode. The MS parameters were optimized as follows: source temperature, 100 °C; desolvation temperature, 400 °C; desolvation gas flow, 500 L h^{-1}; and argon gas flow 50 L h^{-1} was used as the collision gas. The capillary voltage was set at 3.5 kV, the multiplier was set at 650 V, while the cone voltage values for cotinine and IS were 41 and 22 V, respectively. Cotinine and IS were both detected using the multiple reaction mode (MRM) scan, with product ions m/z 349.34 > 305.05 > 249.00, respectively. Measurements were taken in triplicate and data were processed using the MassLynx v.4.0 software.

2.7.2. GEM release studies monitored by fluorescence spectroscopy. To determine GEM release kinetics, suspensions of the nanoparticle's samples were prepared in water at a concertation of 1 mg mL^{-1}, as previously described and they were transferred to a dialysis bag of 3500 kDa MWCO, which was immersed in 3 mL of PBS, of pH 7.4 or pH 5.5, at 37 °C. At predetermined time intervals (30 min, 1 h, 2 h, 4 h, 6 h, 18 h and 24 h), all of the medium was collected and immediately replaced with fresh medium. Again, to evaluate the US effect the experiments were repeated using US after 1 h with a frequency of 1 MHz, a duty cycle of 25% (pulse frequency = 100 Hz) for 5 min and ultrasound power densities of 1.00 and 3.00 W cm^{-2}, or for 30 sec and ultrasound power densities of 2.00 and 4.00 W cm^{-2}. The collected aliquots, of total volume 3 mL each, were processed accordingly the dansyl chloride protocol.[28] A fresh solution of dansyl chloride was prepared by dissolving dansyl chloride in anhydrous DMSO to a final concentration of 10 mg mL^{-1}. For the preparation of the sample, first was add 10 μL of 0.1 M decarbonate buffer, in order to reach pH 9 for the sample, and then 3 μL of dansyl chloride solution was added to the sample. The samples were stirred thoroughly by using a laboratory vortex shake and were incubated at room temperature in the dark for 1–2 h. Before the performance of fluorescence measurement an equal volume of MeOH was added to quench the reaction, as this helps to precipitate any excess of dansyl chloride. Emission spectra in the 300–600 nm range were recorded by exciting the solution at 376 nm and recording the fluorescence intensity at 543 nm. A 5-nm slit was fixed as the width of the excitation and emission light beams. Each sample was analyzed into a quartz QS-cuvette (10 mm) and then excited at 376 nm and the fluorescence intensity was recorded at 543 nm. Measurements were taken in triplicate and data were processed using Matlab software.

2.8. Biological studies

2.8.1. Cell lines and cell culture. The PANC-1 human pancreatic cancer cell lines used were obtained from the European Collection of Cell Cultures-Health Protective Agency ((ECACC-HPA), UK). The cells were cultured and maintained in 25-cm^2 and 75-cm^2 flasks, under standard conditions of normoxia in a humidified atmosphere, at 37 °C, with a 5% (v/v) CO_2 atmosphere. The recommended high glucose DMEM culture media supplemented with 10% (v/v) FBS and 1.1% (v/v) antibiotics (penicillin/streptomycin) were used and changed every 24 h. Then, the cells were harvested by trypsinization in PBS and seeded in 96-well plates for viability assay.

2.8.2. Cytotoxicity assay. The *in vitro* anticancer activity (cytotoxicity/viability) against the PANC-1 cancer cells was investigated by the MTT assay.[29] The cells were seeded into 96-well plates at a density of 0.03 × 10^6 cells per well and allowed to attach and proliferate, under standard conditions, for 24 h. Then, the supernatant in each well was replaced with 300 μL fresh medium containing various concentrations of the samples under investigation. Different groups of the samples were included (a) free drugs of GEM and CPT, (b) NPs, and (c) NP combinations (1 : 1 drug ratio in μM). The concentration range for free GEM and GEM NPs was 1–500 μM, for CPT and CPT NPs was 1.5–290 μM, and for the combinations a window range of 1.5–150 μM was selected. After predetermined time periods of 48 and 72 hours of incubation at 37 °C, the supernatant was completely removed, and the cells were washed with PBS pH 7.4. Then, 180 μL of DMEM and 20 μL of MTT solution (stock 12 mM in PBS pH 7.4) were added in each well, followed by further incubation for 3 h at 37 °C. Then, the medium was completely removed, 150 μL of DMSO were added in each well to dissolve the formazan crystals, and the absorbance was measured at 490 nm (absorbance at a second wavelength of 630 nm was measured also to subtract background noise). The experiments were performed in triplicates and the IC_{50} values were extracted from the dose–effect curves of viability (%) *vs.* concentration (on a log scale).

The same protocol was repeated in order to evaluate the cytotoxicity of all the samples under the effect of US. Three types of treatments were examined: (1) treatment 1: cells incubated first for 24 h in ZnPc rich DMEM (2.8 μM), then DMEM was replaced with fresh ZnPc free medium and the cells were treated with US 22 hours later. 2 hours after US exposure, NPs were added followed by cell viability monitoring at 48 and 72 hours, (2) treatment 2: cells were first cultured for 24 hours followed by simultaneous exposure to ZnPc and NPs for 22 hours; 2 hours later (without changing the medium) they were treated with US followed by cell viability monitoring as previously described and (3) treatment 3: cells were first cultured for 24 hours followed by exposure to ZnPc and NPs for one hour followed by US treatment (again without changing the medium). Each well-plate was treated with US, upon slight immersion in a water bath using a frequency of 1 MHz, a duty cycle of 25% (pulse frequency = 100 Hz) for 3 min and an ultrasound power density of 4 W cm^{-2}. The group of the samples and their concentrations were the same as mentioned above and the experiments were performed in triplicates.

The optical density was assayed in a TECAN infinite F50 spectrophotometer with Gen5 software (Gen5™ Microplate Data Collection & Analysis software, BioTek® Instruments Inc.).

$$\text{Cell viability } \% = \frac{A - B}{C - B} \times 100 \quad (1)$$

where A, B and C are the differences in optical absorbance at 490 and 630 nm of each well containing the formulation, the MTT solution (negative control) and only the cells (positive control), respectively. Data were processed using Matlab software. Student's t-test was used to determine the statistical significance.

2.8.3. Synergism. In order to test synergistic interaction of the PDC combinations, the following two-parameter equation was used.

$$a = \frac{\mathrm{SF}(A) \times \mathrm{SF}(B)}{\mathrm{SF}(\mathrm{combination})} \quad (2)$$

where the number SF is the survival fraction (survival fraction = % metabolic activity/100) for each individual PDC and the SF in the denominator is the survival fraction observed following the combination treatment.[30]

In order to test the synergistic effect of US, ZnPc, and the NPs, a three-parameter equation was used.

$$a = \frac{\mathrm{SF}(\mathrm{combination})}{\mathrm{SF}(A)} + \frac{\mathrm{SF}(\mathrm{combination})}{\mathrm{SF}(B)} + \frac{\mathrm{SF}(\mathrm{combination})}{\mathrm{SF}(C)} \quad (3)$$

where the numbers SF(A), SF(B), SF(C) are the survival fraction (survival fraction = % metabolic activity/100) for each individual "drug" (US, ZnPc, and the PDCs) and the SF in the denominator is the survival fraction observed following the treatment.[30] When $\alpha > 1$, then a synergistic effect has been observed, whereas $\alpha < 1$ denotes an antagonistic effect. $\alpha = 1$ signifies an additive effect of the treatment combination. This analysis has been used previously by others in the field (and beyond) in order to identify the synergistic effects resulting from combinational therapy.[15]

3. Results and discussion

3.1. Polymer prodrug conjugate synthesis

Starting from the commercially available HPMA through esterification we added succinic anhydride to afford a monomer with a slow-reducible linker (**HPMA-Suc**),[31] due to the ester functional group (Fig. 1). The successful synthesis of the modified monomer was confirmed by ^{1}H NMR, with characteristic peaks observed at 2.64–2.66 and 1.88 ppm, corresponding to the hydrogens of the succinic group and to the methyl group of HPMA, respectively (Fig. S1, ESI†). Additionally, ^{13}C NMR showed a distinct peak at 171.47 ppm, attributed to the carbonyl of the ester bond between HPMA and the succinic group (Fig. S2, ESI†). HPMA was selected due to its lower toxicity compared to hydroxyl-group-containing monomers; the cytotoxicity ranking is as follows: 2-hydroxyethyl acrylate (HEEA) > 2-hydroxypropyl acrylate (HPAA) > HPMA > 2-hydroxyethyl methacrylate (HEMA). Additionally, when

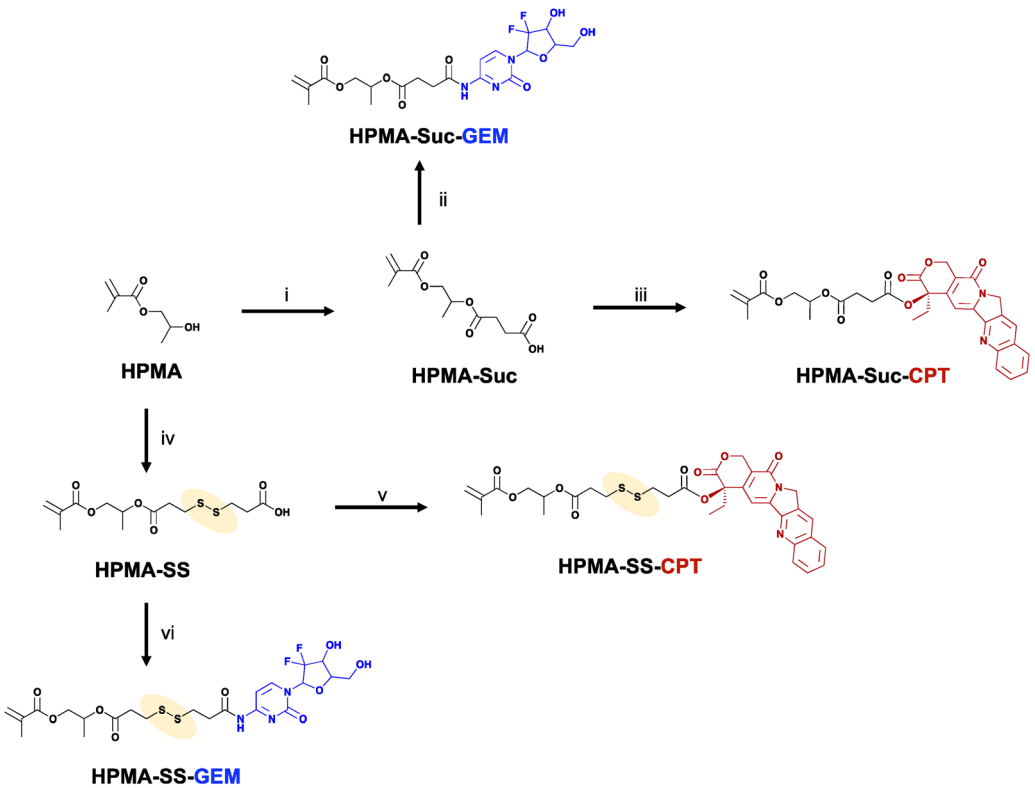

Fig. 1 Synthetic procedure for the monomer prodrugs. Reagents and reaction conditions: (i) succinic anhydride, DMAP, DCM, 30 °C, o/n, under N_2, 49.2%; (ii) GEM, EDCI·HCl, pyridine, DMF, rt, 72 h, under N_2, 39.2%; (iii) CPT, EDCI·HCl, DMAP, DCM, rt, 24 h, under N_2, 80.9%; (iv) DTDP, EDCI·HCl, DMAP, DCM, rt, o/n, under N_2, 49.2%; (v) CPT, EDCI·HCl, DMAP, DCM, rt, 24 h, under N_2, 46%; and (vi) GEM, EDCI·HCl, HOBt, pyridine, DMF, rt, 24 h, under N_2, 47.5%.

comparing the cytotoxicity of HPMA and HEMA with their corresponding alkyl esters, the HPMA alkyl ester exhibits slightly lower toxicity[32] and hence HPMA constitutes the cornerstone starting monomer synthon throughout the study. Then, we used the carboxylic moiety of the modified monomer to attach GEM *via* the amide bond (**HPMA-Suc-GEM**) and CPT *via* an ester bond (**HPMA-Suc-CPT**) with acceptable yields of 40% and 81%, respectively (Fig. 1(ii) and (iii), respectively).[33,34] Both compounds were confirmed by ^{1}H NMR, which showed characteristic aromatic hydrogen signals for each drug (peaks at 7.80 and 7.48 ppm for GEM, and 8.39–7.30 ppm for CPT, Fig. S3 and S5, ESI†). ^{13}C NMR revealed the characteristic peaks of **HPMA-Suc** and the drugs at 172.58 ppm for **HPMA-Suc-GEM**, corresponding to the carbonyl of the amide bond, and at 171.22 ppm for **HPMA-Suc-CPT** (Fig. S4 and S6, ESI†). These NMR findings were further supported by ESI-MS analysis confirming the successful synthesis.

A key issue in our strategy is the choice of the linker, which at later phases will play a critical role during the *in vitro* testing. Disulfide bonds can be easily hydrolyzed in the cell by enzymes and mildly acidic pH (*i.e.*, pH 5.4). Free thiol helps in the hydrolysis of the amide/or ester bond and the subsequent release of the drug.[35] To this end, the prodrug monomers were synthesized in 2 steps, DTDP was first reacted with HPMA to produce an acid functional monomer with a reducible disulfide bond (**HPMA-SS**) (Fig. 1(iv)).[36] The synthesis of **HPMA-SS** was confirmed both by ^{1}H NMR and ^{13}C NMR. ^{1}H NMR confirmed the characteristic peaks at 2.93–2.72 and 1.94 ppm that correspond to DTDP and HPMA, respectively (Fig. S7, ESI†). ^{13}C NMR showed a distinct peak at 171.16 ppm, attributed to the carbonyl of the ester bond between HPMA and DTDP (Fig. S8, ESI†). The acid side chain of this monomer was in turn coupled to the hydroxy group of CPT (**HPMA-SS-CPT**) or the free amine of GEM (**HPMA-SS-GEM**) to form polymerizable prodrug monomers (Fig. 1(v) and (vi), respectively).[33,34] In particular for CPT, the presence of the hydrophobic moiety at the 20S position improves the stability of the lactone towards hydrolysis and decreases the activity under non reducing conditions.[37] Both compounds were confirmed by ^{1}H NMR, which showed characteristic aromatic hydrogen signals for each drug (peaks at 8.49 and 7.46 ppm for GEM, and 8.40–7.28 ppm for CPT, Fig. S9 and S11, ESI†). ^{13}C NMR revealed the characteristic peaks of **HPMA-Suc** and the drugs at 171.23 ppm for **HPMA-SS-GEM**, corresponding to the carbonyl of the amide bond, and at 170.72 ppm for **HPMA-SS-CPT** (Fig. S10 and S12, ESI†). These NMR findings were further supported by ESI-MS analysis.

The polymerizable methacrylate prodrugs were subsequently used as co-monomers in RAFT polymerization. RAFT allows control of the molecular weight and produces well defined polymers with very narrow polydispersity indices ($Đ$ < 1.2). Therefore, we used macroPEG-CTA (M_n = 10 000 g mol^{-1}) in RAFT polymerization with our methacrylate monomer prodrugs in anhydrous DMF at 70 °C for 24 h, in the presence of ACVA as a radical initiator (Fig. 2).

A degree of polymerization (DP) of 50 was chosen as sufficient to induce robust colloidal stability *via* self-assembly and

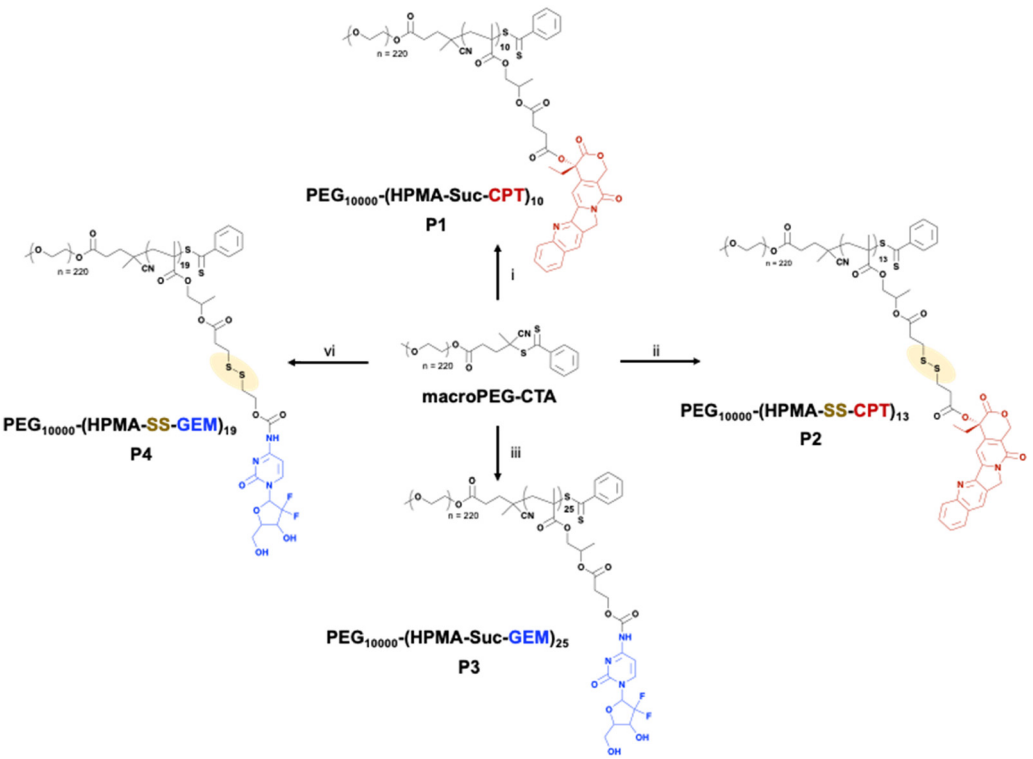

Fig. 2 RAFT polymerization that led to the PDCs. Reagents and general reaction conditions: methacrylate prodrug, ACVA DMF, 70 °C, 24 h, under N_2, (i) 62%; (ii) 60.5%; (iii) 93.6%; and (iv) 60.5%.

Table 1 Polymer characteristics: (a) from SEC (THF, PS standards) and (b) NMR integrals, calculated from the ratio of the monomer to the initiator and macroPEG-CTA to the drug in the NMR spectra

Ref	Polymer	$M_{n,SEC}$[a]	$Đ$[a]	$M_{n,NMR}$[b]	DP[b]	CAC (mg mL^{-1})
P1	PEG-(HPMA-Suc-CPT)$_{10}$	10 800	1.1	15 700	10	0.09
P2	PEG-(HPMA-SS-CPT)$_{13}$	13 400	1.2	18 700	13	0.21
P3	PEG-(HPMA-Suc-GEM)$_{25}$	12 700	1.15	22 200	25	0.12
P4	PEG-(HPMA-SS-GEM)$_{19}$	12 000	1.2	21 000	19	0.22

Table 2 NP characteristics: (a) from DLS and (b) from TEM

NP	D_h (nm)[a]	D_h (nm)[b]	D_h (after 15 days) (nm)[a]	% D_h change[a]	Zeta potential (mV)[a]
P1	312.6 ± 4.8	236.8 ± 30	286 ± 1.5	8.4	0.03 ± 0.07
P2	549 ± 2.5	360.7 ± 41	516.3 ± 8.6	6	0.022 ± 0.005
P3	207 ± 2.6	294.8 ± 76	187.9 ± 2.9	9.2	0.07 ± 0.08
P4	215 ± 2.3	182.13 ± 62	200.8 ± 0.9	6.6	−0.08 ± 0.01
P1 & P2	265 ± 4.8	213 ± 86	196.8 ± 1.7	25.7	0.002 ± 0.027
P3 & P4	226.6 ± 2.6	212.7 ± 55	186.8 ± 3.5	17.6	−0.03 ± 0.05
P1 & P4	593.3 ± 2.3	348.4 ± 49	532.6 ± 2.4	10.2	0.05 ± 0.02
P2 & P3	123.6 ± 2.5	159.8 ± 37	93.5 ± 2.5	24.4	−0.05 ± 0.07

to afford high drug loading with the total mass of the polymer chain for each PDC. The successful synthesis of the PDCs was confirmed by ^{1}H NMR and SEC (Fig. S13–S17, ESI†). It was possible to assign peaks corresponding to the drug molecules (*i.e.*, from 7.89 and 8.35 ppm for GEM and 8.80 to 7.39 ppm for CPT); in addition, the diminishing of the vinyl protons of the methacrylate moieties could be tracked, which confirmed the successful polymerization. The M_n for CPT-rich PDCs was calculated based on integration of 8.80–7.39 ppm peaks and for GEM-rich samples, it was calculated based on 5.26–5.19 ppm peaks (see ESI,† for Fig. S13–S16 for more details). In terms of macromolecular characteristics, M_n values were in the 11 000–13 400 g mol^{-1} range with low dispersities ($Đ$ = 1.1–1.2), suggesting the formation of well-defined samples with good control of the polymerization (Fig. S17, ESI†). Some discrepancy between the M_n values obtained from NMR and SEC is expected as SEC analysis measures the hydrodynamic volume based on the hydrodynamic volume of the calibration standards used, which may be distorted in the mobile phase of the GPC due to the block-copolymer architecture. Hence, for greater accuracy, the DP for all the PDCs was calculated from ^{1}H NMR data (Table 1).

3.2. Nanoparticle formation

The synthesized PDCs could form core–shell types of nanoparticles (NPs) in aqueous media resulting from the block copolymer structure, that is, the hydrophilic PEG and the more hydrophobic drug-rich moieties. NPs were formulated by nanoprecipitation by the drop addition of a $CHCl_3$ solution of PDCs in water followed by the removal of the organic solvent by evaporation. Effective removal of the organic solvent is important for controlling the size of the emergent nanostructures as its presence reduces the stability of the nanoparticles due to Ostwald ripening,[38] in which smaller structures dissociate in order to feed the formation of larger ones.[39] In order to probe the effect of slow and fast drug release we tested different PDC combinations. The formation of colloidally stable self-assembled NPs was confirmed by DLS (Fig. S20–S22, ESI†) and TEM (Fig. S23, ESI†), which were relatively in good agreement (Table 2).

The PDCs generally formed spherical homogenous NP populations with some samples being affected by the presence of large particles, which shifted the overall size distribution towards larger particles (Fig. S22, ESI†). Large NPs could also be traced in the TEM images corroborating the observed size distribution in DLS results. The small difference in diameter values is attributed to the drying effect of the NPs onto the TEM grid. Overall, the particle sizes of the NPs are all relatively large, which can be explained in some formulations (*i.e.*, **P2** and **P1 & P4**) from the distribution of the DLS graphs (Fig. S20 and S22, ESI†), which tend to move D_h to higher numbers. Nevertheless, the sizes of the NPs may be suitable for direct intratumoral injection (*i.e.*, *via* transarterial chemoembolization or catheterization), which could potentially achieve better confinement with a sonosensitizer in a clinical scenario. Furthermore, the stability of the NPs was investigated over time. After 15 days, the D_h values were measured using DLS and were found to be similar to the starting D_h, which is indicative of their good colloidal stability. Interestingly the least stable samples were those made by combining different PDCs (*i.e.*, **P1 & P2**, **P3 & P4**, **P1 & P4**, **P2 & P3**); still the overall stability was adequate with less than 25% change of size at the tested timeframe.

Also, the zeta potential of all the samples is virtually zero, which is expected due to the absence of charged moieties in the molecular structure, implying that the overall stability is solely attributed to the steric effect of the PEG coronae.

3.3. Evaluation of the US effect

First, we conducted preliminary experiments with the PDCs that contain CPT to adjust the time and power of the ultrasound probe. The drug release profiles were found to be non-dependent on US irradiation dose within the window of 30 seconds up to 5 minutes, for a probe power of up to 4 W cm^{-2} (Fig. S24–S27, ESI†).

The release of CPT was performed in neutral (pH 7.4) and acidic (pH 5) aqueous media at 37 °C and monitored by LC-MS/MS. **P1** and **P2** exhibited similar, limited release behavior at pH 7.4, with both showing less than 8% release (Fig. 3a and b). However, under acidic conditions, the release was moderately increased, particularly for **P2,** due to the faster hydrolysis of the disulfide.[35] The presence of Pc was also found to have no effect in the release events for this sample. Overall, the US appears to have an effect under the various conditions evaluated, but the results are unclear because the percentages of the released drug are similar and not distinct enough.

Based on the initial release data, we hypothesized that perhaps the ROS yield from the Pc was relatively low to have an effect on the release profile and we sought to insert a metal

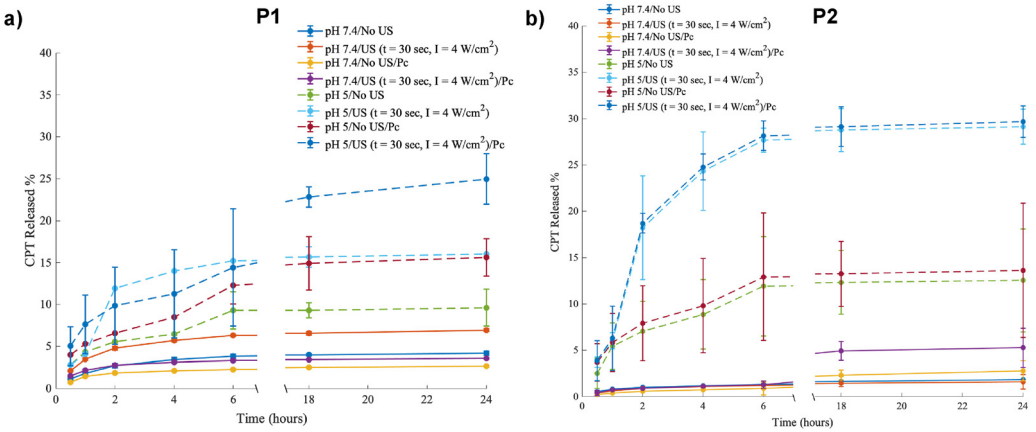

Fig. 3 (a) CPT release of the NPs **P1** and (b) CPT release of the NPs **P2**.

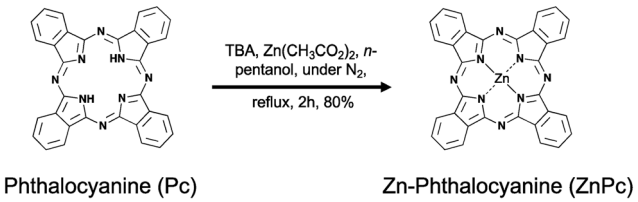

Fig. 4 Metalation reaction of Pc to produce ZnPc.

center in the Pc ring to enhance spin–orbit coupling in favor of higher quantum yield in ROS production (Fig. 4).[22,40] It should be noted that Zn was chosen owing to its proven effect in ROS quantum yield enhancement and its previous use in PDT.[41]

$^1O_2$ is the main component of ROS with biological relevance as it is the main photooxidation product of phototherapies and can be monitored by the DPBF assay. It was confirmed that the metalated ZnPc could generate significantly more $^1O_2$ than the non-metalated under the tested conditions (Fig. S29–S30, ESI†). ZnPc could also generate hydroxyl radicals (•OH) by US irradiation as evidenced by the TA assay, which acts as a selective •OH radical trap producing the UV-vis measurable product N A (Fig. 5a).[42–45]

Fig. 5b compares the ability of Pc and ZnPc to generate ROS, including •OH, with ABS normalized to the maximum value. In the DBPF assay, the absorbance of DBPF decreases as $^1O_2$ is produced (Fig. 5a). The change in absorbance (ΔABS = ABS at 0 min – ABS at 60 min) for Pc is only 2%, compared to 32% for ZnPc, demonstrating a significantly enhanced ROS generation capacity for ZnPc. In the TA assay, absorbance increases as •OH generates more HTA. To evaluate the •OH production, the ΔABS (ABS at 60 min – ABS at 0 min) was calculated, yielding 30% for ZnPc and 12% for Pc. Overall, ZnPc exhibits a superior ability to generate ROS, which translates to enhanced drug release in release experiments. While Pc slightly enhances drug release, ZnPc significantly increases the release rate (see release profiles in Fig. 7).

It is well known that US can induce the formation of •OH in water, in a similar way as ionizing radiation. Since •OH is a major free-radical intermediate and an important precursor for many products formed by the action of US in aqueous

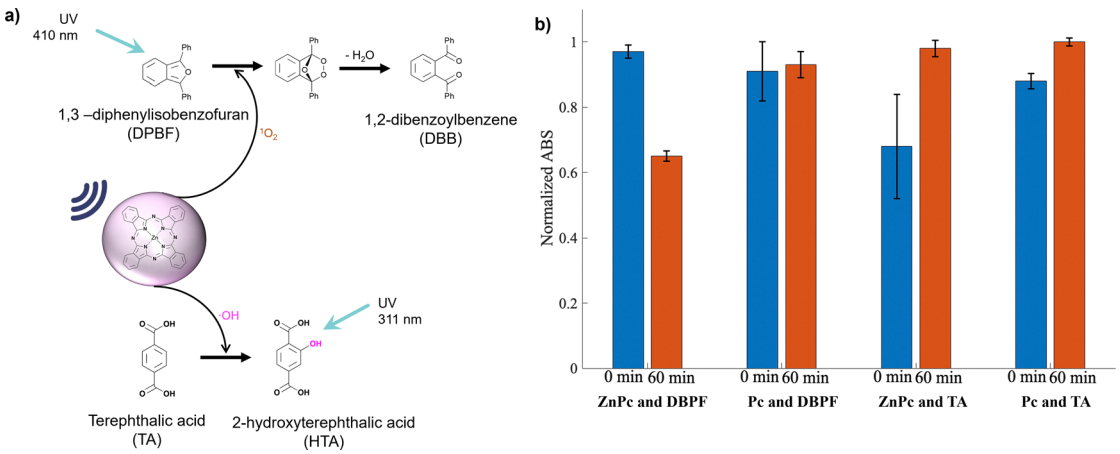

Fig. 5 (a) Photo-oxidation of DPBF by $^1O_2$ and the formation of HTA *via* the reaction of TA and •OH and (b) quenching of DPBF and generation of HTA by US irradiation in the presence of Pc or ZnPc.

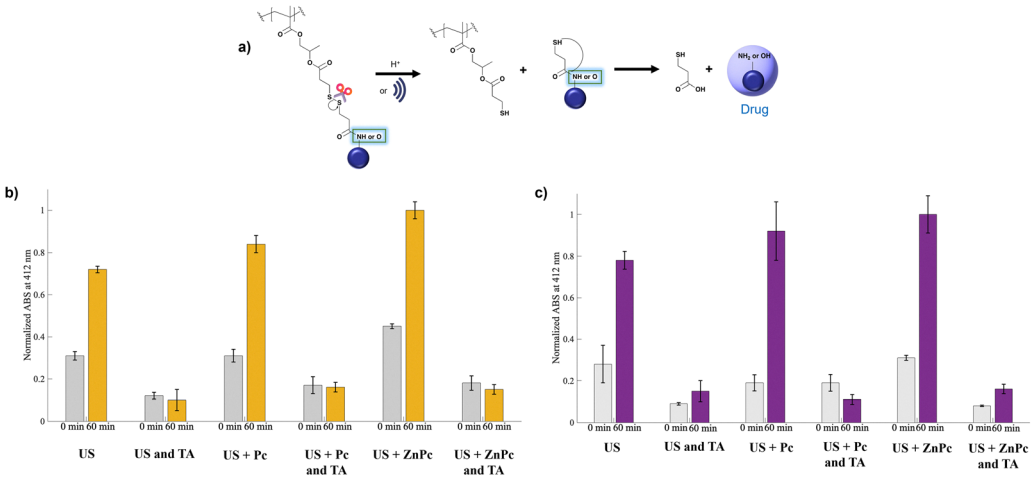

Fig. 6 (a) Hydrolysis of the disulfide bond, (b) Ellman's assay for **P2**, and (c) Ellman's assay for **P4**.

solutions, •OH can also have a critical role in the breakage of the disulfide bond (Fig. 6a).[43]

The effect of US and the use of Pc or ZnPc was verified using Ellman's assay with the normalized ABS with the highest ABS values (Fig. 6b and c). In the presence of free thiols, an absorbance at 412 nm is observed due to the chromogenic 5-nitro-2-thiobenzoic acid (TNB). Both **P2** and **P4** contain a disulfide linker with either CPT or GEM, respectively. US promotes the breakage of this disulfide bond, as confirmed by the release studies (Fig. 3a and b). The presence of Pc further enhances this effect, with an even greater enhancement observed with ZnPc. To investigate the role of •OH, experiments were conducted in the presence of TA, a scavenger used to trap •OH. In these experiments, no absorbance was recorded at 412 nm, indicating that the disulfide bond did not break and highlighting the critical role of •OH in bond cleavage. Furthermore, Fig. 5b shows that Pc produces less $^1O_2$ and •OH compared to ZnPc, which explains the larger TNB peak at 412 nm with ZnPc.

As ZnPc has enhanced production of ROS, release experiments were conducted for all PDCs in the presence of ZnPc at a fixed US dose. Generally, the presence of Zn seems to enhance the rate of release across the samples. At pH 7.4, CPT release from **P1** exhibited similar rates in the presence and absence of Pc (Fig. 3a and 7a). The presence of ZnPc did not significantly improve the drug release even at acidic pH, which remained at 35%. However, at acidic pH, for **P2** a clear difference was observed between experiments with Pc and ZnPc. With Pc, the maximum release rate of CPT reached 30%, whereas with ZnPc, the total release of CPT was 80% (Fig. 7b).

At pH 7.4, the GEM release was consistently low (<10%) across all conditions. However, at pH 5, GEM release increased in the presence of ZnPc, reaching nearly 20%, whereas without ZnPc, GEM release remained similar to the levels observed at pH 7.4 (Fig. 7c). Notably, at pH 5, the highest GEM release was achieved when ultrasound was applied, following a similar trend as in CPT. To assess the effect of US on the disulfide linker, we repeated release experiments with **P4** with and without the presence of ZnPc (Fig. S27a and b, ESI†). As expected, at pH 7.4 the release was very low; the highest rate was 10%, which was reached at 4 W cm^{-2} of US (Fig. 7c). At acidic pH the release was significantly higher with US (*ca.* 40%) and increased by 25% with ZnPc (Fig. 7d). From this set of experiments, we conclude that US combined with ZnPc has a significant impact on the release events at acidic pH across all samples. The release seems to be affected in the first 6–7 hours followed by steady state release later as monitored up to 24 hours.

A notable distinction lies in the extent of drug release: while CPT achieves near-complete release under the tested conditions; GEM exhibits a controlled release profile. This attenuated release behavior suggests enhanced modulation of drug delivery, potentially attributable to differences in chemical bond stability. Specifically, CPT is conjugated *via* an ester bond, which is comparatively labile under hydrolytic conditions, facilitating rapid cleavage and full release.[46] In contrast, GEM is linked through a more stable amide bond, which resists hydrolysis and delays drug liberation.[46] The enhanced stability of the amide bond likely prolongs retention of GEM within the nanocarrier, enabling sustained, controlled release. This mechanistic distinction underscores the importance of bond selection in tailoring drug delivery profiles for therapeutic precision.

3.4. *In vitro* cell studies

3.4.1. Treatment modalities. In order to find the optimum combination of treatment, three types of treatment modalities were investigated (Fig. 8). In treatment 1, the cells were first pretreated with ZnPc to ensure sufficient insertion into the cytosol, and the US was applied after 22 h. After 2 h the NPs were added, to further minimize viability. In the second modality treatment, the cells were pretreated with a combination of ZnPc and NPs followed by US after 22 h. Treatment 3 was similar to treatment 2, but no pretreatment was followed since the US was applied only 1 h after incubation with the combination of ZnPc and NPs. In all treatments the intensity of the

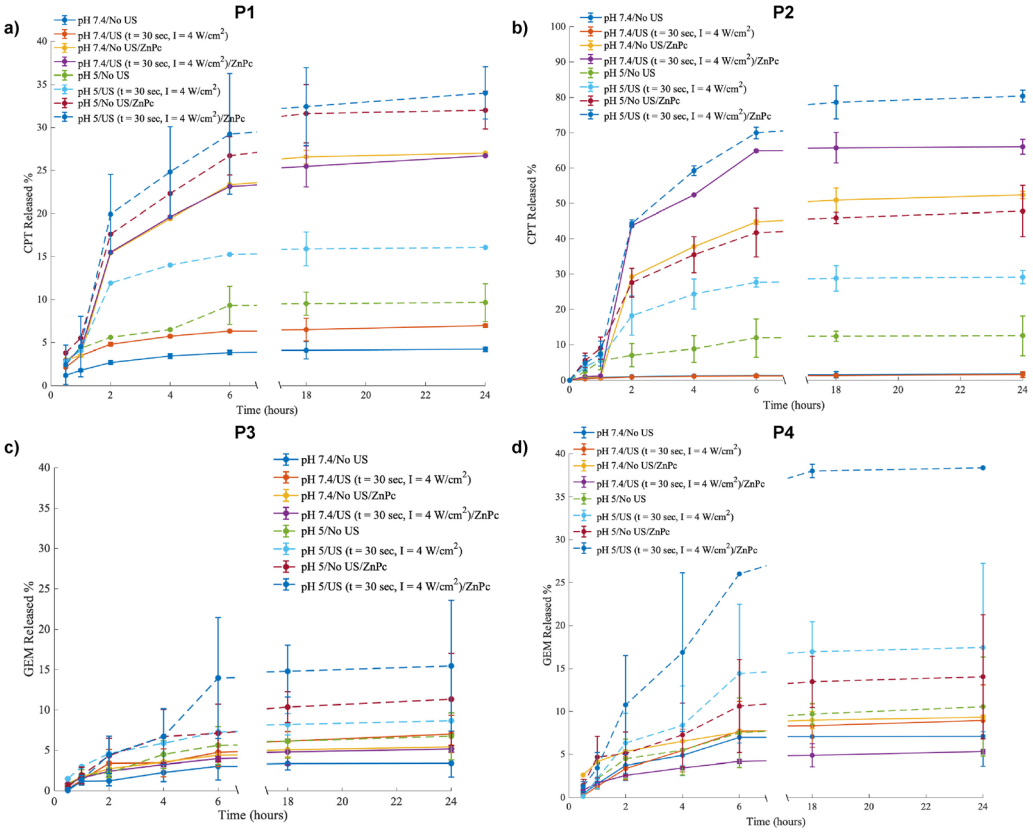

Fig. 7 (a) Release profile of the NPs **P1**, (b) release profile of the NPs **P2**, (c) release profile of the NPs **P3** and (d) release profile of the NPs **P4**.

US was 4 W cm^{-2} for 3 min, as these conditions were not found to influence the viability of the cells (Fig. S31, ESI†).

3.4.2. Cytotoxicity evaluation of the NPs. All NPs with and without the presence of ZnPc were tested for cytotoxicity against PANC-1 cells as a clinically relevant model for assessing the cytotoxicity of GEM and CPT. Free drugs and their respective PDC combinations of all linkers at a CPT : GEM molar ratio of 1 : 1 were also evaluated. Cytotoxicity was evaluated at 48 (Fig. S32, ESI†) and 72 h (Fig. 9), which generally showed a similar trend across the samples. However, the overall cytotoxic effect was more pronounced at 72 h, as GEM and CPT reach their maximum therapeutic potential over time. This delay occurs because CPT must penetrate the nucleus, while GEM, as a prodrug, requires activation *via* phosphorylation pathways to exert its effects.[47]

The IC_{50} values of free CPT and GEM were 154 ± 4 μM and 254 ± 4 μM, respectively (Fig. 9a and b), which were considerably higher than those reported in the literature (107.6 nM for CPT[48] and 10 nM for GEM[49]). This suggests that the cell line used in our study exhibits resistance to both frontline chemotherapeutics GEM and CPT, while common drug resistant PANC-1 cells exhibit an IC_{50} value of 50 μM for GEM.[50] An

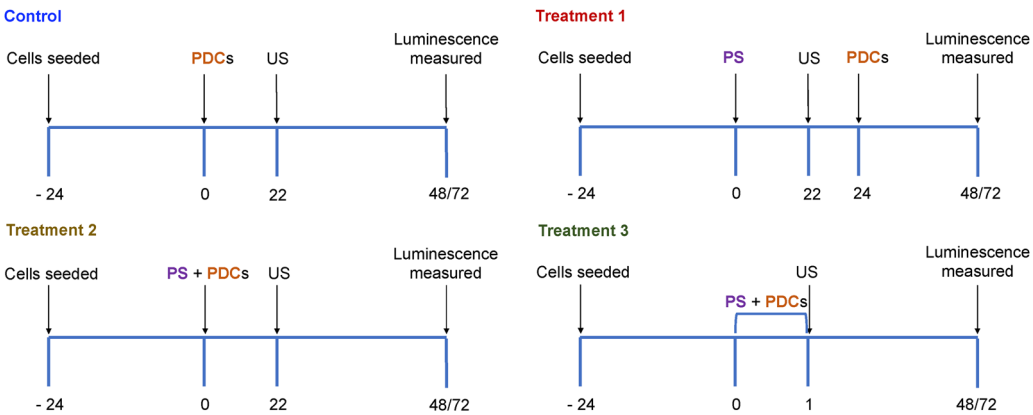

Fig. 8 Different treatment modalities.

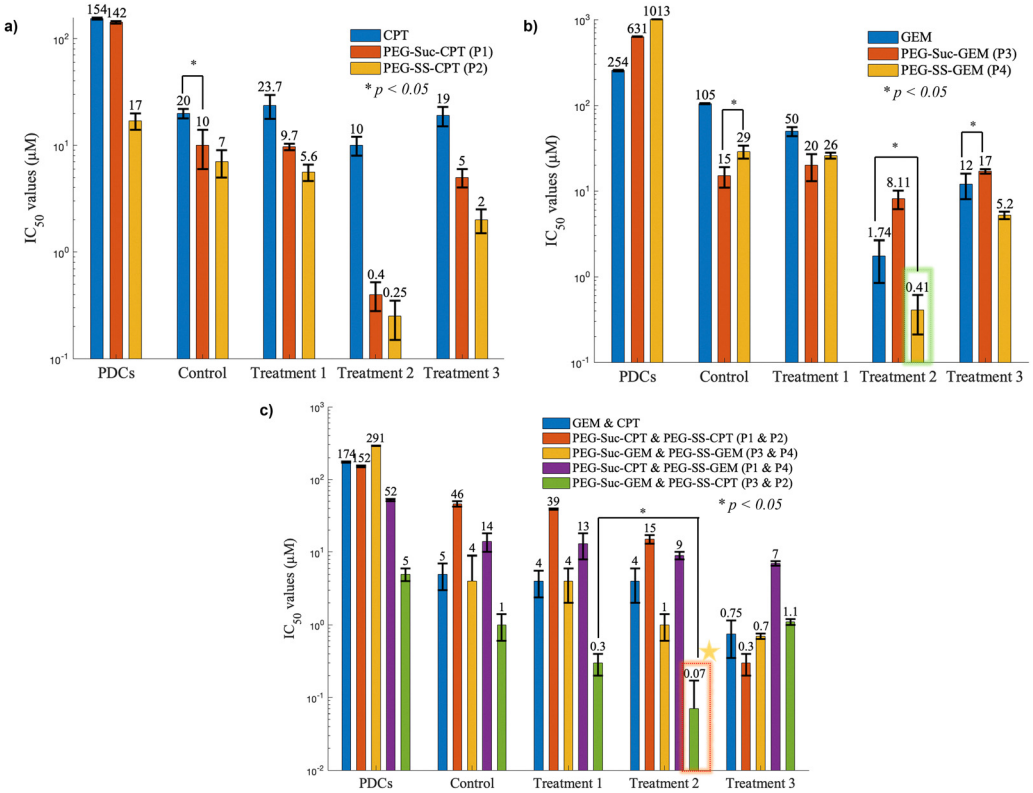

Fig. 9 IC_{50} values of (a) free CPT, NPs **P1** and **P2**, (b) free GEM, NPs **P3** and **P4**, and (c) their combinations: GEM + CPT, PEG-Suc-CPT & PEG-SS-CPT (**P1 & P2**), PEG-Suc-GEM & PEG-SS-GEM (**P3 & P4**), PEG-Suc-CPT & PEG-SS-GEM (**P1 & P4**), and PEG-Suc-GEM & PEG-SS-CPT (**P3 & P2**).

interesting observation is that while GEM PDCs (**P3** and **P4**) exhibited higher IC_{50} values (631 ± 4 μM for **P3** and 1013 ± 3 μM for **P4**), expectedly indicating reduced cytotoxicity, CPT NPs (**P1** and **P2**) showed lower IC_{50} values compared to the parent drug (142 ± 4 μM for **P1** and 17 ± 3 μM for **P2**). This suggests that the CPT free drug may have undergone hydrolysis of the lactone ring prematurely within the cells, leading to a reduced cytotoxic effect;[51] the polymer scaffold could possibly have a protective effect of premature hydrolysis events in this scenario. In comparison with previous studies,[52] where low IC_{50} values have been reported in absence of any additional treatment, our GEM and the CPT-ester NPs seem to exhibit reduced cytotoxic efficacy, as reflected by their higher IC_{50} values. This implies that they exert a safer (*i.e.*, less toxic) therapeutic profile if not activated, that is if US is not applied. Interestingly, the presence of ZnPc under treatment 2 protocol resulted in the most favorable IC_{50} values (5 ± 0.2 μM for **P1**, 2 ± 0.7 μM for **P2**, 8.11 ± 2 μM for **P3**, and 0.41 ± 0.12 μM for **P4**), outperforming all other treatments (Fig. 9). In contrast, treatment 1 showed reduced cytotoxicity, likely because the effect was primarily driven by radicals produced from ZnPc, which were not expected to enhance cytotoxicity significantly as shown in control experiments (Fig. S34, ESI†). Meanwhile, treatment 3 exhibited significantly lower IC_{50} values compared to treatment 1, but the shorter time of cells exposur to PDCs before US application was insufficient for sufficient cellular uptake, unlike treatment 2. Treatment 2 exhibited the most potent IC_{50} values, likely due to the adequate time allowed for ZnPc and the PDCs to internalize into the cells and, with the co-assistance of US, showed a significantly more potent therapeutic effect.

In order to evaluate the role of the different linkers, four PDC combinations were tested: combinations with the same drug (CPT or GEM) but different linkers and combinations with mixed linkers and drugs. These combinations were selected to investigate how linker chemistry and drug pairings influence the release kinetics and therapeutic efficacy of the PDCs, providing insights into optimizing drug delivery strategies. The most potent combination was **P2 & P3**, with the IC_{50} value being 5 ± 1 μM (Fig. 9c). Remarkably, upon application of US in the presence of ZnPc (treatment 2 protocol) a 71-fold decrease in cell viability was observed, with an IC_{50} value of 0.07 ± 0.1 μM (Fig. 9c) far exceeding the potency of the parent drugs and their combinations, by 5 orders of magnitude. Presumably this result is the outcome of the quick response of CPT (disulfide linked) and the slower but systemic exposure of the cells with GEM (ester linked), leading to an overall enhanced therapeutic effect at 72 hours. This pattern is significantly augmented by the co-treatment with ZnPc.

In our previous work, where we evaluated the toxicity of GEM-nanomedicines activated by laser rather than US, an IC_{50} of 0.5 μM was achieved in the MiaPaCa-2 cell line.[15] This is significantly higher than the lowest IC_{50} observed in this study (0.07 ± 0.1 μM for **P2 & P3**), highlighting the enhanced potency

of our drug-delivery system. Moreover, it is important to note that the PANC-1 cell line used in this study is resistant, further underscoring the therapeutic potential of our approach.

3.4.3. Synergy effect. To elucidate whether there is any synergism across the samples and their combinations we calculated the synergism parameter for each group of samples tested using the Chou-Talalay method (*i.e.*, for samples, **GEM & CPT**, **P1 & P2**, **P3 & P4**, **P1 & P4**, and **P3 & P2**).[53] Generally, the combinations showed an antagonistic effect ($\alpha < 1$), while at 25 μM, α reached values closer to 1 for the combination of free drugs (GEM and CPT), and **P3** and **P2**, indicating the additive effect of the drugs (Fig. S35, ESI†). Conversely, the combination of GEM with the different linkers (**P3 & P4**) showed a nearly synergistic effect ($\alpha > 1$) at a concentration of 25 μM, and at the same concentration, the combination of GEM-ester with CPT-disulfide linkers (**P3 & P2**) showed an additive effect ($\alpha = 1$).

To evaluate the synergistic effect of the combination of US, ZnPc, and the PDCs, we determined the synergy parameter for treatment 2 (eqn (3)),[30] which showed the best IC_{50} values out of all treatments. At low concentrations, all PDCs (Fig. 10a) and their combinations (Fig. 10b) demonstrated a synergistic effect. However, at higher concentrations, the effect shifted toward a borderline antagonistic and additive effect. This trend at higher concentrations can be attributed to the antagonistic effects observed in the absence of US and ZnPc. If the drugs alone were synergistic, the synergy effect would probably have been further enhanced. Moreover, given that the applied US intensity and ZnPc alone were not toxic, and the PDCs had greater IC_{50} values than the parent drugs, implies that their combination appears to yield an enhanced therapeutic outcome—consistent with the IC_{50} values obtained.

Although synergism studies are of limited phenomenological interpretation of the PDC combinations under the different treatment protocols, they can provide effective guiding in the optimization of potent therapeutic modalities that consist of multiple parameters (*i.e.*, drug cocktails, external triggering mechanisms, *etc.*). For example, CIs as feedback readouts may provide guiding in focusing parameters (US intensity, ZnPc dose, or treatment duration, drug combinations, *etc.*) that will clearly impact the *in vitro* response and lead to optimization of the treatment modalities in future studies.

Finally, to investigate the efficacy of the treatments, we compared the E_{max} value, which is indicative of a treatment's efficacy and represents the value of cell viability at the maximum tested drug concentration (here, 1000 μM). The key treatment effects, indicative of treatment potency and efficacy (IC_{50}; E_{max}), were identified from the chemotherapy (that is, without US) and the sonochemical (that is, ZnPc with US) cytotoxicity profiles for each drug and their combinations and are summarized in Table 3 (for chemotherapy and treatment 2) and Table S1 (ESI†) (for US, treatment 1, and treatment 3). Chemotherapy and sonochemical therapy effects were also compared with each other, and the corresponding changes in potency and efficacy are also listed. The most potent sonochemical therapy is treatment 2, with **P1**, **P1 & P2**, and **P1 & P4** being the most efficacious, exhibiting a 6.7, 2.3, and 3.1-fold increase compared to sole chemotherapy, respectively. Notably, **P4** demonstrates a remarkable ~2470-fold improvement in its

Table 3 IC_{50} and E_{max} values comparing the treatment effects of chemotherapy with treatment 2 by drug class

Drug	Treatment	IC_{50} (μM)	Fold improvement	E_{max} (% control) [±SE]	Efficacy change (fold)
CPT	Chemotherapy	154		42 (±6)	
P1		142		40 (±7)	
P2		17		43 (±9)	
GEM		254		40 (±2)	
P3		631		50 (±4)	
P4		1013		50 (±6)	
GEM & CPT		174		32 (±2)	
P1 & P2		152		41 (±6)	
P3 & P4		291		46 (±1)	
P1 & P4		52		25 (±5)	
P2 & P3		5		31 (±5)	
CPT	Treatment 2	10	+15.4	39 (±1)	+1.1
P1		0.4	+355	6 (±14)	+6.7
P2		0.25	+68	28 (±3)	+1.5
GEM		1.74	+146	17 (±7)	+2.3
P3		8.11	+77.8	33 (±3)	+1.5
P4		0.41	+2471	36 (±9)	+1.4
GEM & CPT		4	+43.5	12 (±11)	+2.7
P1 & P2		15	+10.1	18 (±4)	+2.3
P3 & P4		1	+294	26 (±2)	+1.8
P1 & P4		9	+5.8	8 (±2)	+3.1
P2 & P3		0.07	+71.4	43 (±2)	−0.7

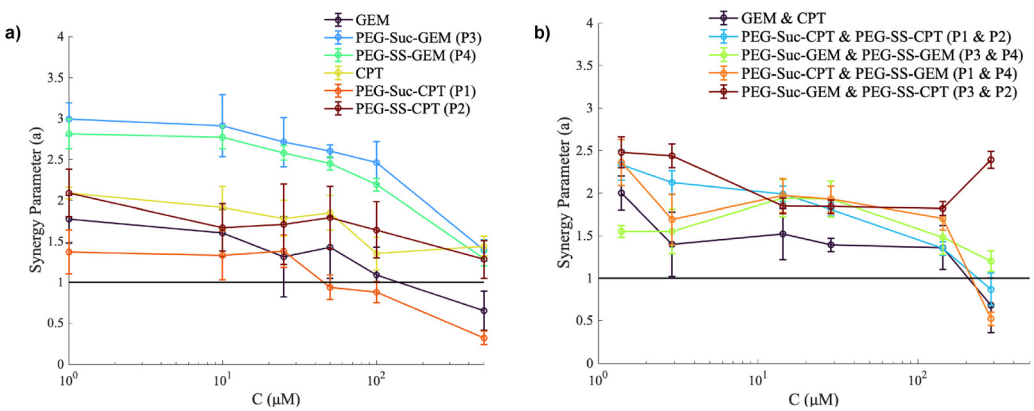

Fig. 10 Synergy parameter for treatment 2: (a) NPs from a single polymer type and (b) NPs from a combination of two polymers.

IC_{50} value (0.41 μM in treatment 2 compared to 1013 μM in chemotherapy). In contrast, while the combination of **P2 & P3** achieves the lowest IC_{50} value (0.07 μM in treatment 2 *vs.* 5 μM in chemotherapy), its fold improvement is less pronounced due to the already low IC_{50} in chemotherapy.

To address the feasibility of translating this platform to clinical settings and the safety profile of ZnPc and PDCs, several factors must be considered. First of all, the feasibility to access pancreatic tumors with ultrasound probes has been shown in clinical studies.[54–58] Potentially, US treatment could be accompanied by the co-delivery of PDCs by direct injection to achieve effective accumulation of drug molecules at the site of treatment. This is critical if one considers the presence of a sonosensitizer to fully harness the benefit of US in drug release events as shown in this study. Confinement of the different drug molecules is another critical factor that must be fulfilled to maximize the therapeutic effect as seen by the combination indexes. Co-formulation strategies with spatially controlled US treatment may be a potent approach that exerts aggressive cytotoxicity while minimizing side effects in non-irradiated areas. This is clearly shown in Fig. S34 (ESI†) where ZnPc and PDCs exhibit minimal cytotoxicity in the absence of US activation, indicating a potentially safer therapeutic profile when not triggered. This can be further enhanced by direct delivery of PDCs at the tumor sites, which eliminates the exposure of healthy tissues to PDCs.

4. Conclusions

This study demonstrated the successful synthesis and characterization of PDCs designed for pancreatic tumor-targeted drug delivery. By employing tailored linker chemistries, we achieved controlled and stimuli-responsive drug release profiles, emphasizing the importance of disulfide bonds in enhancing the release kinetics under acidic conditions and in response to US application. The incorporation of ZnPc significantly improved ROS production, further enhancing the release efficacy of CPT and GEM from the formulations. To evaluate the role of different linkers, four PDC combinations were tested, combinations with of the same drug, CPT or GEM, but different linkers and combinations with mixed linkers and drugs, to investigate how linker chemistry and drug pairings influence release kinetics and therapeutic efficacy, thereby optimizing drug delivery strategies. These findings underline the interplay between linker chemistry, formulation parameters (*e.g.*, drug combinations), and US treatment protocols; particularly, PDC pretreatment timing critically influences cytotoxicity against resistant PANC-1 cell lines, with IC_{50} values as low as 0.07 ± 0.1 μM for optimized combinations (*e.g.*, **P2 & P3** under the treatment 2 protocol). This represents a key result of our study for *in vitro* data evaluation in that NP pretreatment can support a critical cascade of biological events promoting anticancer activity. This is a key message not just for our study but for any study that reports *in vitro* data, in that incubation and US treatment timing play a significant role in biological events and it is always worth exploring possible blind spots that can be revealed by harnessing subtle experimental variations while testing the disease protocol. Finally, in porphyrin activated therapeutics (be they of photochemical or sonodynamic nature), the choice of the porphyrin molecule is absolutely key to fully exploit the potential of any RATM; in this study, we used the simplest phthalocyanine, which already showed enhanced ROS generation *via* metalation; however, the overall effect could be further enhanced by increasing its amphiphilic character as we have shown in our previous studies.[15] All in all, it is clear that sonochemical RATMs utilizing PDC combinations constitute a potent concept that, if carefully used, can lead to highly cytotoxic outcomes with extremely high ΔIC_{50} (that is, fold-improvement) at the activated areas.

Author contributions

Dimitra Toumpa: conceptualization, writing – original draft, validation, methodology, investigation, formal analysis, experimental design, and data collection and curation; Athina Angelopoulou: reviewing and editing, methodology and *in vitro* data analysis; Konstantinos Avgoustakis: reviewing and editing, resources, methodology; and George Pasparakis: writing – reviewing and editing, writing – original draft, validation, supervision, resources, project administration, methodology, investigation, funding acquisition, formal analysis, data curation, conceptualization.

Conflicts of interest

There are no conflicts to declare.

Data availability

The data of the manuscript are available through the University of Patras repository at the websites **https://www.polylab.gr** and **https://www.upatras.gr**. All data are also available at OSFHOME under the project ''ultrasound nanomedicines'' at the URL: **https://osf.io/6rbhj/**.

Acknowledgements

This work was supported by the Hellenic Foundation for Research and Innovation (H.F.R.I., project ULTRAMED No. 00234). We thank Alexandros Kyriakos Bikogiannakis and Prof. Georgios Kyriakou (Department of Chemical Engineering, University of Patras) for the XPS measurements and analysis. We thank Prof. Michael Kornaros (Department of Chemical Engineering, University of Patras) for the access to the UV-vis spectrometer, Prof. Theodoros Christopoulos (Department of Chemistry, University of Patras) for providing access to the spectrofluorometer and Prof. Theodore Tselios (Department of Chemistry, University of Patras) for the access to ESI-MS. We thank Dr Mohamed A. El Mubarak and Prof. Gregory B. Sivolapenko (Department of Pharmacy, University of Patras)

for conducting the LC-MS/MS measurements. The Instrumental Analysis Laboratory (School of Natural Sciences, University of Patras) is gratefully acknowledged for carrying out the NMR analysis. The Laboratory of Electron Microscopy and Microanalysis (Department of Biology, University of Patras) for imaging is kindly acknowledged.

References

1 H. Hu, P. Busa, Y. Zhao and C. Zhao, *Smart Mater. Med.*, 2024, **5**, 386–408.
2 D. V. Voronin, A. A. Abalymov, Y. I. Svenskaya and M. V. Lomova, *Int. J. Mol. Sci.*, 2021, **22**, 9149.
3 S. Mura, J. Nicolas and P. Couvreur, *Nat. Mater.*, 2013, **12**, 991–1003.
4 A. Zhang, K. Jung, A. Li, J. Liu and C. Boyer, *Prog. Polym. Sci.*, 2019, **99**, 101164.
5 X. Zhao, J. Liu, J. Fan, H. Chao and X. Peng, *Chem. Soc. Rev.*, 2021, **50**, 4185–4219.
6 G. Gunaydin, M. E. Gedik and S. Ayan, *Front. Chem.*, 2021, **9**, 691697.
7 J. H. Correia, J. A. Rodrigues, S. Pimenta, T. Dong and Z. Yang, *Pharmaceutics*, 2021, **13**, 1332.
8 W. Jerjes, T. A. Theodossiou, H. Hirschberg, A. Høgset, A. Weyergang, P. K. Selbo, Z. Hamdoon, C. Hopper and K. Berg, *J. Clin. Med.*, 2020, **9**, 528.
9 D. Costley, C. Mc Ewan, C. Fowley, A. P. McHale, J. Atchison, N. Nomikou and J. F. Callan, *Int. J. Hyperthermia*, 2015, **31**, 107–117.
10 I. Rosenthal, J. Z. Sostaric and P. Riesz, *Ultrason. Sonochem.*, 2004, **11**, 349–363.
11 Y. Zhang, X. Zhang, H. Yang, L. Yu, Y. Xu, A. Sharma, P. Yin, X. Li, J. S. Kim and Y. Sun, *Chem. Soc. Rev.*, 2021, **50**, 11227–11248.
12 M. H.-C. Lin, L.-C. Chang, C.-Y. Chung, W.-C. Huang, M.-H. Lee, K.-T. Chen, P.-S. Lai and J.-T. Yang, *Pharmaceutics*, 2021, **13**, 1877.
13 H. Maemoto, R. Suzaki, K. Watanabe, K. Itaka and T. Ohtsuki, *Eur. J. Med. Chem. Rep.*, 2025, **13**, 100242.
14 H.-L. Lu, W.-J. Syu, N. Nishiyama, K. Kataoka and P.-S. Lai, *J. Controlled Release*, 2011, **155**, 458–464.
15 C. Barnett, F. Joubert, A. Iliopoulou, R. S. Álvarez and G. Pasparakis, *Mol. Pharmaceutics*, 2023, **20**, 1818–1841.
16 G. Pasparakis, T. Manouras, M. Vamvakaki and P. Argitis, *Nat. Commun.*, 2014, **5**, 3623.
17 P. Thakor, V. Bhavana, R. Sharma, S. Srivastava, S. B. Singh and N. K. Mehra, *Drug Discovery Today*, 2020, **25**, 1718–1726.
18 I. Ekladious, Y. L. Colson and M. W. Grinstaff, *Nat. Rev. Drug Discovery*, 2019, **18**, 273–294.
19 J. Wu, *J. Pers. Med.*, 2021, **11**, 771.
20 S. Tsatsos, S. Ladas and G. Kyriakou, *J. Phys. Chem. C*, 2020, **124**, 26268–26278.
21 C. D. Wagner, L. E. Davis, M. V. Zeller, J. A. Taylor, R. H. Raymond and L. H. Gale, *Surf. Interface Anal.*, 1981, **3**, 211–225.
22 I. M. Denekamp, F. L. P. Veenstra, P. Jungbacker and G. Rothenberg, *Appl. Organomet. Chem.*, 2019, **33**, e4872.
23 A. Singh, S. Malhotra, D. Bimal, L. M. Bouchet, S. Wedepohl, M. Calderón and A. K. Prasad, *ACS Omega*, 2021, **6**, 103–112.
24 S. O. McDonnell, M. J. Hall, L. T. Allen, A. Byrne, W. M. Gallagher and D. F. O'Shea, *J. Am. Chem. Soc.*, 2005, **127**, 16360–16361.
25 B. Tang, L. Zhang and Y. Geng, *Talanta*, 2005, **65**, 769–775.
26 A. Habeeb, *Methods in enzymology*, Elsevier, 1972, vol. 25, pp. 457–464.
27 Z. Wang, C. Shao, Z. Hu, J. Zheng, Q. Zhang, X. Kou, Z. Wang, T. Yu, Z. Cao and Y. Wang, *J. Pharm. Biomed. Anal.*, 2020, **179**, 112963.
28 W. R. Gray, *Methods Enzymol.*, 1967, **11**, 139–151.
29 T. Mosmann, *J. Immunol. Methods*, 1983, **65**, 55–63.
30 T.-C. Chou, *Pharmacol. Rev.*, 2006, **58**, 621–681.
31 K. J. Takafumi Nakayama, FUJFILM Corporation, Tokyo (JP), 2020, US 2020/0115316 A1, 28.
32 E. Yoshii, *J. Biomed. Mater. Res.*, 1997, **37**, 517–524.
33 L. Xiao, Y. Zhou, X. Zhang, Y. Ding and Q. Li, *Chem. Pharm. Bull.*, 2019, **67**, 1082–1087.
34 F. Joubert and G. Pasparakis, *J. Mater. Chem. B*, 2018, **6**, 1095–1104.
35 Z. Shi, J. Wu, Q. Song, R. Göstl and A. Herrmann, *J. Am. Chem. Soc.*, 2020, **142**, 14725–14732.
36 Z. T. W. H. L. X. B. H. W. Jiafeng, CN202110428510 20210421, 2021.
37 M.-J. Li, C. Jiang, M.-Z. Li and T.-P. You, *J. Mol. Struct. THEOCHEM*, 2005, **723**, 165–170.
38 V. Kumar and R. Prud'homme, *Chem. Eng. Sci.*, 2009, **64**, 1358–1361.
39 A. G. Cheetham, R. W. Chakroun, W. Ma and H. Cui, *Chem. Soc. Rev.*, 2017, **46**, 6638–6663.
40 J. Karolczak, D. Kowalska, A. Lukaszewicz, A. Maciejewski and R. P. Steer, *J. Phys. Chem. A*, 2004, **108**, 4570–4575.
41 T. D. de Souza, F. I. Ziembowicz, D. F. Müller, S. C. Lauermann, C. L. Kloster, R. C. Santos, L. Q. Lopes, A. F. Ourique, G. Machado and M. A. Villetti, *Eur. J. Pharm. Sci.*, 2016, **83**, 88–98.
42 J. C. Barreto, G. S. Smith, N. H. P. Strobel, P. A. McQuillin and T. A. Miller, *Life Sci.*, 1994, **56**, PL89–PL96.
43 X. Fang, G. Mark and C. von Sonntag, *Ultrason. Sonochem.*, 1996, **3**, 57–63.
44 S. E. Page, W. A. Arnold and K. McNeill, *J. Environ. Monit.*, 2010, **12**, 1658–1665.
45 D. H. Gonzalez, X. M. Kuang, J. A. Scott, G. O. Rocha and S. E. Paulson, *Anal. Lett.*, 2018, **51**, 2488–2497.
46 A. Dal Corso, L. Pignataro, L. Belvisi and C. Gennari, *Chemistry*, 2019, **25**, 14740–14757.
47 E. Moysan, G. Bastiat and J.-P. Benoit, *Mol. Pharmaceutics*, 2013, **10**, 430–444.
48 S. Park, J. Sung, E. Kim and N. Chung, *Braz. J. Med. Biol. Res.*, 2014, **48**, 111–119.
49 D. P. Jeansonne, G. Y. Koh, F. Zhang, H. Kirk-Ballard, L. Wolff, D. Liu, K. Eilertsen and Z. Liu, *Oncol. Rep.*, 2011, **25**, 1473–1480.

50 H. Kakwere, E. S. Ingham, S. K. Tumbale and K. W. Ferrara, *Mater. Sci. Eng., C*, 2020, **117**, 111251.
51 M. Ghanbari-Movahed, T. Kaceli, A. Mondal, M. H. Farzaei and A. Bishayee, *Biomedicines*, 2021, **9**, 480.
52 K. Kaliya, N. Bhardwaj, Ruchika and A. Saneja, *ChemMedChem*, 2025, **9**, 8.
53 T.-C. Chou, *Cancer Res.*, 2010, **70**, 440–446.
54 T. Inui, H. Amitani, K. Kubo, D. Kuchiike, Y. Uto, T. Nishikata and M. Mette, *Anticancer Res.*, 2016, **36**, 3767–3770.
55 T. Inui, K. Makita, H. Miura, A. Matsuda, D. Kuchiike, K. Kubo, M. Mette, Y. Uto, T. Nishikata and H. Hori, *Anticancer Res.*, 2014, **34**, 4589–4593.
56 Y. Jiang, J. Fan, Y. Li, G. Wu, Y. Wang, J. Yang, M. Wang, Z. Cao, Q. Li and H. Wang, *Int. J. Cardiol.*, 2021, **325**, 132–139.
57 A. Bunevicius, S. Pikis, F. Padilla, F. Prada and J. Sheehan, *J. Neuro-Oncol.*, 2022, **156**, 1–10.
58 A. Sofuni and T. Itoi, *J. Med. Ultrason.*, 2022, DOI: **10.1007/s10396-022-01263-x**.

